X-ray Analysis and Molecular Modeling of Poly(vinyl alcohol)s with Different Stereoregularities

J. D. Cho, W. S. Lyoo,† S. N. Chvalun,‡ and J. Blackwell*

Department of Macromolecular Science, Case Western Reserve University, Cleveland, Ohio 44106-7202

Received May 28, 1999; Revised Manuscript Received July 29, 1999

ABSTRACT: Wide-angle X-ray methods have been used to compare the structures of poly(vinyl alcohol) (PVA) with syndiotactic diad (S-diad) contents in the range 51−63%. The fiber diagram of a PVA with 51.2% S-diad content (essentially atactic) is indexed by a monoclinic unit cell with dimensions $a = 7.82 \pm 0.03$ Å, $b = 2.53 \pm 0.01$ Å (chain axis), $c = 5.52 \pm 0.01$ Å, and $\beta = 91.5 \pm 0.2°$. These dimensions are very similar to those proposed by Bunn (*Nature* **1948**, *161*, 929) and Sakurada (*Bull. Inst. Chem. Res., Kyoto Univ.* **1950**, *23*, 78). As the S-diad content is increased, the crystallites become larger and less distorted and there is lateral contraction of the crystal structure, suggesting that the chains can pack more efficiently. For a syndiotacticity-rich PVA with a S-diad content of 63.1%, the unit cell dimensions are as follows: $a = 7.63 \pm 0.02$ Å, $b = 2.54 \pm 0.01$ Å, $c = 5.41 \pm 0.01$ Å, and $\beta = 91.2 \pm 0.1°$. The latter structure has a theoretical density of 1.40 g/mL, which is ∼5% higher than the value of 1.34 g/mL predicted for the atactic polymer. The efficiency of chain packing in the two unit cells has been compared by molecular dynamics modeling of arrays of chain segments of different random sequences, with 50% and 65% S-diad contents. For both structures, the results favor hydrogen bonding similar to that proposed by Bunn rather than that due to Sakurada. *NVT* calculations show that the larger unit cell is favored for the atactic polymer, while the smaller unit cell is favored for the 65% syndiotactic polymer. A *NPT* assembly for the atactic model starting in the contracted unit cell expanded and equilibrated close to the observed, lower density structure. Likewise, a starting model for the 65% syndiotactic polymer packed with the dimensions for the atactic polymer was found to adjust to the observed contracted structure. The changes are to be understood in terms of the balance between hydrogen bonds (electrostatic) and van der Waals forces, which vary depending on the tacticity.

Introduction

Atactic poly(vinyl alcohol) (PVA) prepared by saponification of poly(vinyl acetate) is distinctly crystalline despite its lack of stereoregularity.[1−3] X-ray fiber diagrams point to a planar zigzag backbone conformation with an advance per monomer in the region of 2.52 Å. Bunn[1,3] indexed the observed Bragg reflections with a monoclinic unit cell with the following dimensions: $a = 7.81$ Å, $b = 2.52$ Å (chain axis), $c = 5.51$ Å, and $\beta = 91.42°$, containing single monomer units of two chains. These dimensions have been confirmed in several later analyses.[4−9] The *ac* projection of the model proposed by Bunn is shown in Figure 1a, and this illustrates the possible hydrogen bonding for the two monomer configurations. The unit cell describes an average structure (copolymer) in which each monomer has half hydroxyls at the two possible positions. An alternative packing arrangement has been proposed by Sakurada et al.[2] in which the chains have a different setting angle and the hydrogen bonds point along the *a* axis, as shown in Figure 1b.

Recently there has been interest in the production of high performance fibers based on high molecular weight (HMW) syndiotacticity-rich PVA, which have mechanical and physical properties that are superior to those of preparations of the atactic polymer.[10−15] This improvement is ascribed to the higher crystallinity due to the increased stereoregularity. In our laboratories, it was found that oriented microfibrils of PVA were formed during saponification of poly(vinyl pivalate) (PVPi).[16,17] Control of the molecular weight and stereoregularity was achieved by saponification of copolymers of vinyl pivalate (VPi) and vinyl acetate (VAc). Depending on the comonomer ratio and the concentration of initiator (2,2′-azobis(2,4-dimethylvaleronitrile)), the PVAs obtained had number-average molecular weights in the range $(2.47−7.26) \times 10^5$ (DP = $(5.6−16.5) \times 10^3$) and syndiotactic diad (S-diad) contents of 52.8−61.5%. The highest molecular weight and S-diad content were obtained for specimens derived from the VPi homopolymer prepared at low initiator concentration, and these parameters declined progressively with increasing VAc content in the parent copolymer. Interestingly, the structures of these PVAs show a consistent transition between ∼55 and 57% S-diad contents. Specimens with lower S-diad contents have shapeless morphologies, but above 56% S-diad content, the polymers have a fibrous

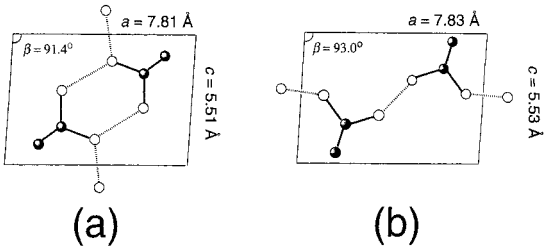

Figure 1. *ac* projection of the crystal structure of atactic PVA proposed by (a) Bunn,[1] and (b) Sakurada.[2] (dark circle, carbon; white circle, oxygen; dashed line, hydrogen bond).

* To whom correspondence should be addressed. Telephone: (216) 368-6370. Fax: (216) 368-4202. E-mail: jxb6@po.cwru.edu.
† Present address: School of Textiles, Yeungnam University, Kyongsan 712-749, Republic of Korea.
‡ Permanent Address: Polymer Structure Laboratory, Karpov Institute of Physical Chemistry, Ul. Vorontsovo Pole 10, Moscow, 103064, Russia.

10.1021/ma9908402 CCC: $18.00
Published on Web 09/03/1999

morphology with higher degrees of crystallinity. The order improves steadily as the S-diad content increases further, and it correlates with observed changes in the thermal and mechanical properties.

In the present paper, we have used X-ray diffraction to compare the structure of four PVAs with S-diad contents of 51.2%, 54.5%, 58.4%, and 63.1%, to investigate the effect of increased stereoregularity on the chain packing and hydrogen bonding. It will be seen that there is a contraction of the lateral dimensions of the unit cell with increasing S-diad content, leading to an increase in density of the ordered regions. Molecular modeling has been applied to these structures to probe the energetics of the chain packing as the tacticity is increased.

Experimental Section

PVA Specimens. PVAs with S-diad content 51.2%, 54.5%, 58.4%, and 63.1% were obtained by saponification of PVPi or PVAc, as described by Lyoo et al.[16] The specimens with 63.1% and 58.4% S-diad content consisted of fibrillated mats, from which individual fibrils could be teased. Fibers of the PVAs with 54.5% and 51.2% S-diad content were produced by dry-jet wet spinning: PVA (5% w/v) was dissolved in a 50/50 (v/v) mixture of dimethyl sulfoxide and water mixture at 120 °C under nitrogen to prevent oxidative degradation. Dry-jet spinning was performed by extrusion through a nozzle of diameter 0.8 mm, into air at 30−60 °C, and the product was coagulated in methanol at −20 °C. Zone drawing of the gel-spun fibers at 225 °C was performed using an Instron model 4201, with crosshead speeds ranging from 10 to 200 mm/min to achieve maximum draw ratio.

X-ray Diffraction. Wide-angle X-ray diffraction (WAXD) data for aligned bundles of PVA fibers were recorded under vacuum on Kodak Direct Exposure film using pinhole collimation and Ni-filtered Cu Kα radiation. The *d* spacings were calibrated using CaF_2 powder. $\theta/2\theta$ diffractometer scans of PVA fibers were recorded on a Phillips PN 3550 diffractometer equipped with a scintillation counter, operated in the transmission mode with a constant slit width of $^1/_{12}°$ using Ni-filtered Cu Kα radiation. The data were collected at 2θ increments of 0.02°, with a counting time of 30 s. The crystallite size perpendicular to the chain axis direction was estimated from the integral peak widths (δ) for the *h*00 reflections, using silicon powder as the standard in order to correct for instrumental broadening. The extent of paracrystalline distortion was estimated using a modified Hosemann equation[18]

$$\delta = 1/L_{hkl}^2 + (\pi g n)^2/d_{hkl}^2 \qquad (1)$$

where L_{hkl} is the mean dimension of the crystallite perpendicular to the *hkl* plane, d_{hkl} is the interplanar spacing, *n* is the order of the reflection, and *g* is the paracrystallinity index ($g = \langle \Delta d_{hkl} \rangle / d_{hkl}$), and $\langle \Delta d_{hkl} \rangle$ is the standard deviation for the distribution of interplanar spacings.

Model Building. Atomic models of PVA were constructed using the bond lengths C−C = 1.54 Å, C−O = 1.43 Å, C−H = 1.10 Å, and O−H = 0.95 Å, and bond angles C−C−*C* = C−C−O = C−C−H = C−O−H = 109.5°, which are compatible with those derived from X-ray data.[5] The chain backbones had the planar zigzag conformation, with a repeat of 2.52 Å. The hydrogen of the hydroxyl group was arranged *trans* to the methine hydrogen. Atomic charges were calculated using the Gasteiger-Hückel method.

Hydrogen-terminated PVA chains with 50% and 65% S-diad contents were constructed with sequences determined using a random number generator. Arrays of nonidentical parallel chains were constructed for crystal structure models based on the unit cell for atactic PVA proposed by Bunn, with lateral dimensions $a = 7.81$ Å, $c = 5.51$ Å, and $\beta = 91.82°$, and on the "contracted" unit cell observed for the PVA with 63.1% S-diad content, which had dimensions $a = 7.63$ Å, $c = 5.41$ Å, and $\beta = 91.5°$. The first chain had its backbone through *a*/4, *c*/4 with the methine C−H bond pointing along the *ac* diagonal, with a setting angle of 35.15° for the Bunn unit cell and 34.90° for the contracted unit cell. (0° is when the *b* axis projection of the backbone C−C bonds coincides with the *a* axis and positive angles correspond to counterclockwise rotation.) In each case, the second chain was generated from the first by a rotation of 180° about the *b* axis and a translation to *a*/2, *b*/2, *c*/2, as in the structure proposed by Bunn (Figure 1a).

Molecular Mechanics (MM). Here, 8 × 6 arrays of chains of 40 monomers (total 1920 monomers, 13 536 atoms) were subjected to energy minimization using the SYBYL force field.[19] Four models were constructed: 50% and 65% S-diad contents packed in both the Bunn and contracted unit cells. Hereafter, these models are referred to as Bunn 50, Bunn 65, contracted 50, and contracted 65. A periodic boundary condition (PBC) was applied in each case, using dimensions $a = 31.24$ Å, $b = 103.3$ Å, $c = 33.00$ Å, and $\beta = 91.8°$ for the Bunn models and $a = 30.52$ Å, $b = 103.3$ Å, $c = 32.40$ Å, and $\beta = 91.5°$ for the contracted models.

Molecular Dynamics (MD). Here, 4 × 2 arrays of chains of 12 monomers (total 96 monomers, 688 atoms) were constructed in the same way as above, for Bunn and contracted unit cells with both 50% and 65% S-diad contents. They were subjected to energy minimization and MD simulation using Insight II software (MSI, San Diego, CA). Modeling using the CVFF, CFF91, and ESFF force fields from the Discover program[20] showed that CVFF resulted in unit cell dimensions closest to those observed, and CVFF was used in all simulations. (In these calculations, hydrogen bonds are treated as a natural consequence of the van der Waals and electrostatic parameters.) Monoclinic PBCs were applied as for the MM calculations. The simulations used a combination of the steepest decent and conjugated gradient methods, until the energy difference converged to less than 0.001 kcal/mol. The atom-based cutoff distance was 9.5 Å (real space spline distance up to 8.5 Å) for both van der Waals (vdW) and electrostatic forces. We set the dielectric constant at 1, and applied the Verlet velocity integrator. The choice of a 9.5 Å cutoff distance with the spline switching method[20] was arbitrary. However, test experiments showed that use of higher cutoff distances (up to 30 Å) had relatively little effect on the final total energy and the actual refined structure. This probably arises from the relatively distorted structures of the copolymer arrays, which is such that the O···O and O···H distance correlation functions become smooth at separations greater than ∼10 Å.

Constant temperature and constant volume (*NVT*) ensembles were used to compare structures packed in the observed unit cells; constant temperature and constant pressure (*NPT*) ensembles were used to obtain preferred unit cell dimensions for arrays of the different S-diad contents. Energies were evaluated at increments of 1 fs and saved every 10 fs. The energy of the final models were averaged over 10 ps at 298 K after 20 ps of equilibration for the *NVT* ensembles and over 50 ps at 298 K and 1 atm after 50 ps of equilibration for the *NPT* ensembles.

Results and Discussion

X-ray Diffraction. Figure 2 shows the X-ray fiber diagrams for the four specimens of PVA with different tacticities. All four specimens have high orientation of the chains along the fiber axis direction. Superficially the crystallinity appears high in all cases, and the Bragg reflections sharpen as the S-diad content increases: the 101 and $10\bar{1}$ reflections are easily resolved when the S-diad content is 63.1%. The *d* spacings of the observed reflections for the four specimens are given in Table 1. It is seen that the reflections on the different layer lines show a systematic trend toward lower *d* spacings as the S-diad content increases. This is apparent in Figure 3 which shows the $\theta/2\theta$ diffractometer scans along the

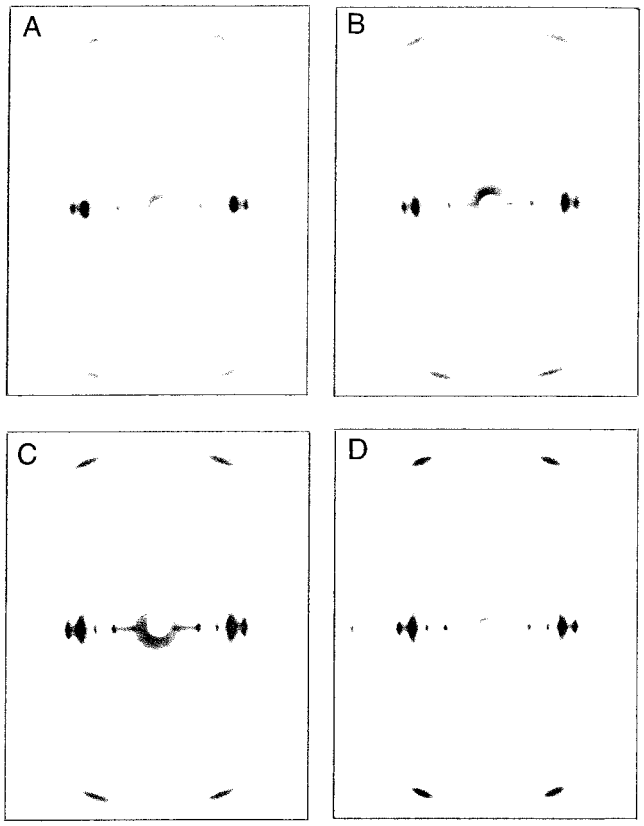

Figure 2. Wide-angle X-ray fiber diagrams of PVAs with different S-diad contents: (a) 51.2%; (b) 54.5%; (c) 58.4%; and (d) 63.1%.

Table 1. Observed *d* Spacings (Å) for the Four PVAs with Different Syndiotacticities

51.2% S-diad	54.5% S-diad	58.4% S-diad	63.1% S-diad
	Equatorial		
7.86 ± 0.04	7.85 ± 0.04	7.77 ± 0.03	7.63 ± 0.03
5.54 ± 0.03	5.54 ± 0.03	5.53 ± 0.02	5.41 ± 0.02
4.59 ± 0.03	4.60 ± 0.02	4.56 ± 0.02	4.45 ± 0.02
4.45 ± 0.02	4.46 ± 0.02	4.42 ± 0.02	4.37 ± 0.02
3.91 ± 0.02	3.92 ± 0.02	3.94 ± 0.02	3.82 ± 0.02
3.25 ± 0.02	3.25 ± 0.02	3.23 ± 0.02	3.17 ± 0.02
3.12 ± 0.02	3.11 ± 0.02	3.10 ± 0.02	3.10 ± 0.02
2.76 ± 0.02	2.75 ± 0.02	2.74 ± 0.02	2.70 ± 0.02
2.58 ± 0.02	2.59 ± 0.02	2.58 ± 0.01	2.55 ± 0.01
2.31 ± 0.01	2.30 ± 0.01	2.32 ± 0.01	2.27 ± 0.01
2.21 ± 0.01	2.20 ± 0.01	2.22 ± 0.01	2.18 ± 0.01
1.94 ± 0.01	1.94 ± 0.01	1.94 ± 0.01	1.92 ± 0.01
1.81 ± 0.01	1.82 ± 0.01	1.82 ± 0.01	1.79 ± 0.01
1.65 ± 0.01		1.67 ± 0.01	1.61 ± 0.01
	First Layer (off Meridional)		
2.44 ± 0.02	2.44 ± 0.02	2.43 ± 0.03	2.44 ± 0.02
2.21 ± 0.02	2.22 ± 0.02	2.22 ± 0.01	2.20 ± 0.01
2.13 ± 0.01	2.13 ± 0.01	2.13 ± 0.01	2.14 ± 0.01
	Second Layer (Meridional)		
1.26 ± 0.01	1.27 ± 0.01	1.26 ± 0.01	1.27 ± 0.01

equatorial direction through the 100, 001, 10$\bar{1}$, and 101 reflections; the peaks sharpen and shift to higher scattering angle with increasing syndiotacticity, such that the *d* spacings decrease by ~2%.

Refinement of the unit cell parameters based on the data in Table 1 yields the following dimensions: a = 7.63 ± 0.02 Å, b = 2.54 ± 0.01 Å, c = 5.41 ± 0.01 Å, and β = 91.2 ± 0.1° for 63.1% S-diad content and a = 7.82 ± 0.03 Å, b = 2.53 ± 0.01 Å, c = 5.52 ± 0.01 Å, and β = 91.5 ± 0.2° for 51.2% S-diad content. The good agreement between the observed and calculated *d* spacings is demonstrated in Table 2. The dimensions for 51.2% S-diad content are similar to those proposed by Bunn[1] and Sakurada.[2] Thus, increasing S-diad content from 51.2 to 61.3% has resulted in a 2−2.5% lateral contraction of the *a* and *c* dimensions of the unit cell; the fiber repeat, *b*, and the monoclinic angle, β, are essentially unchanged. The measured densities of the specimens with 51.2 and 63.1% S-diad contents are 1.33 and 1.38 g/mL, respectively. These data compare well with calculated densities of 1.34 and 1.40 g/mL, respectively, based on two monomers per unit cell.

Lateral and longitudinal crystallite sizes were derived from the integral breadth of the *h*00 and 020 reflections, respectively, and are listed in Table 3. We observed three orders of *h*00 reflections, and these data were used to derive the lateral crystallite sizes corrected for paracrystalline distortion. Plots of δ vs n^2 were approximately linear, and Table 3 shows the corrected lateral crystallite sizes and the indices of paracrystallinity. The lateral crystallite size increases from 110 ± 5 Å for 51.2% S-diad content to 214 ± 10 Å at 63.1% S-diad content, while g falls from 2.77 ± 0.09% to 1.37 ± 0.05%. At the same time, the axial crystallite size increases progressively from 103 ± 7 to 143 ± 10 Å respectively. Thus, the change in tacticity leads to a reduction in the unit cell volume, i.e., a higher density, and the crystallites increase in size and perfection.

The most striking of the above observations is that the lateral packing becomes much tighter as the S-diad content increases from 51.2 to 63.1%. At 51.2% S-diad content we have essentially the atactic polymer, which is nevertheless highly crystalline: the pendant hydroxyl groups can be accommodated in both configurations. In the structure proposed by Bunn, the chains have a planar zigzag conformation and the hydroxyl groups on adjacent monomer units on the center and origin chains in the unit cell are linked by hydrogen bonds. Thus, to a first approximation, the lattice separation of the chains is determined by a compromise between the attraction due to hydrogen bonding and the van der Waals steric repulsions between the adjacent monomers. When the S-diad ratio is changed, these two effects would be expected to balance at a different interchain separation; i.e., the optimum unit cell dimensions should change. We have used molecular modeling techniques to address this problem, as is described below.

Molecular Modeling. Molecular Mechanics (MM). Table 4 shows the total energies, and their components, due to van der Waals, electrostatic, torsional effects, etc., for the four arrays after 500 minimization iterations. The energy of the starting Bunn 50 model was 21 773 kcal/mol compared to 43 995 kcal/mol for the contracted 50 model; that for the Bunn 65% model was 28 653 kcal/mol compared to 52 797 kcal/mol for the contracted 65 model. These energies are all unacceptably high due to van der Waals overlap, which inherently is worse in the contracted unit cells. However, the energies all reduced to negative values on minimization, when the overlap was eliminated mainly as a result of changes in the torsional angles at the backbone C−C bonds. After minimization, the Bunn 50 model had a lower energy (−7244.1 kcal/mol) than for the contracted 50 model (−7018.5 kcal/mol), although the difference is only 0.12 kcal·mol^{-1}/monomer. The average backbone torsion angle deviated from 180° (trans) by only 0.3°, with a standard deviation of 7.5°, indicating that only minor backbone distortion had occurred. Contraction of the

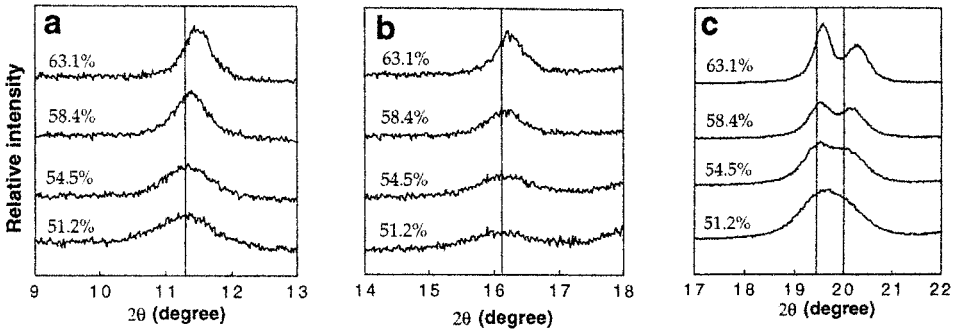

Figure 3. Equatorial diffractometer scans of fibers of the four PVA specimens: (a) 100, (b) 001, and (c) $10\bar{1}$ and 101 reflections. The vertical lines indicate the scattering angle (2θ) predicted for Bunn model.

Table 2. Comparison of the Observed and Calculated *d* Spacings (Å) for PVAs with 51.2% and 63.1% Syndiotacticity

51.2% S-diad			63.1% S-diad		
obsd	calcd	*hkl*	obsd	calcd	*hkl*
7.86 ± 0.04	7.81	100	7.63 ± 0.03	7.63	100
5.54 ± 0.03	5.51	001	5.41 ± 0.02	5.41	001
4.59 ± 0.03	4.56	$10\bar{1}$	4.45 ± 0.02	4.46	$10\bar{1}$
4.45 ± 0.02	4.44	101	4.37 ± 0.02	4.37	101
3.91 ± 0.02	3.90	200	3.82 ± 0.02	3.81	200
3.25 ± 0.02	3.22	$20\bar{1}$	3.17 ± 0.01	3.15	$20\bar{1}$
3.12 ± 0.02	3.14	201	3.10 ± 0.01	3.08	201
2.76 ± 0.02	2.75	002	2.70 ± 0.02	2.70	002
2.58 ± 0.02	2.60	300	2.55 ± 0.01	2.54	300
2.31 ± 0.01	2.33	301	2.27 ± 0.01	2.28	301
2.21 ± 0.01	2.22	202	2.18 ± 0.01	2.18	202
1.94 ± 0.01	1.95	400	1.92 ± 0.01	1.91	400
1.81 ± 0.01	1.84	003	1.79 ± 0.01	1.80	003
	1.82	401		1.79	401
1.65 ± 0.01	1.64	203	1.61 ± 0.01	1.62	203
2.44 ± 0.02	2.52	010	2.44 ± 0.02	2.54	010
	2.40	110		2.41	110
2.21 ± 0.02	2.19	111	2.20 ± 0.02	2.22	111
2.13 ± 0.01	2.12	210	2.14 ± 0.01	2.11	210
1.26 ± 0.01	1.26	020	1.27 ± 0.01	1.27	020

Table 3. Lateral and Axial Crystalline Widths (*L*) for PVAs with Different Tacticities

S-diad (%)	51.2	54.5	58.4	63.1
L_{h00} (Å)	110 ± 5	128 ± 6	173 ± 8	214 ± 10
g (%)	2.77 ± 0.09	2.43 ± 0.08	1.69 ± 0.06	1.37 ± 0.05
L_{0k0} (Å)	103 ± 7	116 ± 8	135 ± 10	143 ± 10

The table also includes the lateral paracrystalline index (g).

lateral dimensions to those of the smaller unit cell led to a reduction in the electrostatic component, as a result of the shorter hydrogen bonds, but this reduction was exceeded by the increase in the vdW term due to close O···O contacts. After energy minimization of the models with 65% S-diad content, the contracted 65 model had the higher energy (−6340.7 kcal/mol) than that for the Bunn 65 model (−6665.5 kcal/mol), but again the energy difference is small (0.17 kcal·mol^{-1}/monomer). The average backbone torsion angle deviated by 0.3° from 180°, with a standard deviation of 9.2°. The energy differences between the Bunn and contracted models are very small, and in any case, plots of energy vs iteration number suggested that the structures were not fully minimized after 500 iterations. We concluded that global minima have not been achieved, and that molecular mechanics is unlikely to resolve the differences between the expanded and contracted unit cells. We therefore proceeded to molecular dynamics simulations in order to address this question.

Molecular Dynamics (MD). Constant Volume and Temperature (*NVT*). Because of the size of the computations necessary for the MD simulations, we used smaller arrays than those used for molecular mechanics: 8 chains, each of 12 monomers of random sequence. Figure 4 shows the potential energies of the four models plotted against with time during *NVT* simulations. The total energies and the contributions from nonbonded and electrostatic interactions are listed in Table 5. The major effects of hydrogen bonding are to be seen in the electrostatic term.

The potential energies decreased initially and then fluctuated over constant average values, indicating that all structures had equilibrated within this time frame. After 30 ps at 298 K, the potential energies were ∼3.1 kcal·mol^{-1}/monomer lower than those for the equivalent MM minimizations. Figure 5 shows projections of the Bunn 50 model along the fiber axis direction: (a) before minimization, (b) after MM energy minimization, and (c) after 30 ps MD (*NVT*). The bond lengths and bond angles for all four final structures were in reasonable accord with literature values (within 0.58 and 3.65% rms, respectively). For 50% S-diad content, the total energy for the Bunn 50 model is −3948.6 kcal/mol, which is lower than the value of −3924.9 kcal/mol for the contracted 50 model (0.25 kcal/mol monomer). For 65% syndiotacticity, the total energy for the Bunn 65 model is −3909.4 kcal/mol compared to −3925.6 kcal/mol for contracted 65 model (0.17 kcal/mol monomer). So the observed unit cells correspond to models with the lower energies. The energy differences are in line with what one might expect for structures that differ in terms of hydrogen bond lengths.

Lateral cell contraction of the models for 65% S-diad content leads to increase of ∼58 kcal/mol in the vdW energy while the electrostatic energy is reduced by ∼72 kcal/mol. The latter effect suggests the formation of stronger hydrogen bonds. For the atactic models, contraction of the lateral dimensions reduced the electrostatic term as a result of the shorter hydrogen bonds, but this reduction is exceeded by the increase in the vdW term due to closer O···O contacts between adjacent monomers, as occurred in MM simulations. For the contracted 50 model, the electrostatic energy is ∼65 kcal/mol lower than that for the Bunn 50 model. However, contraction has also induced significantly more angle bending ($\Delta E_{\text{angle}} = 0.17$ kcal·mol^{-1}/monomer) and torsional distortion ($\Delta E_{\text{dist}} = 0.24$ kcal·mol^{-1}/monomer) than occurs for the contracted 65 model. These data suggest that unit cell contraction for atactic PVA would lead to bad contacts between monomers of opposite configuration, and avoidance of the vdW overlap results in backbone distortion. Once overlap of the

Table 4. Potential Energies and Their Components for the Four Packing Models Following Molecular Mechanics Minimization

	atactic		65% syndiotactic	
	Bunn 50	contracted 50	Bunn 65	contracted 65
total energy (kcal·mol^{-1})	−7244.1	−7018.5	−6665.5	−6340.7
ΔE (kcal·mol^{-1}/monomer)	0.118		0.169	
bond stretching	238.5	208.3	217.0	195.1
angle bending	801.9	863.3	854.5	921.7
torsional	512.1	591.4	695.4	776.8
1,4-van der Waals	1125.3	1222.5	1197.8	1286.0
van der Waals	−7286.1	−7047.8	−7114.4	−6811.3
1,4-electrostatic	−3617.7	−3636.0	−3602.6	−3620.8
electrostatic	985.2	779.9	1086.9	911.8

Table 5. Total Energies (and Their Components) for the Four Packing Models Following Molecular Dynamics Calculations (*NVT* Ensembles) at 298 K with Fixed Unit Cell Dimensions

	atactic		65% syndiotactic	
	Bunn 50	contracted 50	Bunn 65	contracted 65
total energy (kcal·mol^{-1})	−3948.6	−3924.9	−3909.4	−3925.6
ΔE (kcal·mol^{-1}/monomer)	0.25		0.17	
potential energy	−4558.6	−4534.8	−4519.2	−4535.1
kinetic	609.9	609.9	609.9	610.0
electrostatic	−5481.7	−5546.1	−5450.3	−5522.6
van der Waals	103.9	156.3	39.6	98.0
dispersive-vdW	−1439.6	−1544.3	−1403.0	−1514.6
repulsive-vdW	1543.4	1700.6	1442.6	1612.6
bond	270.4	266.4	289.2	281.5
angle	443.8	460.4	483.3	490.6
torsion	105.0	128.2	119.0	117.3

Table 6. Predicted Unit Cell Dimensions[a] for the Four Packing Models Following Molecular Dynamics Calculations (*NPT* Ensembles) at 298 K and 1.013 bar

	atactic		65% syndiotacticity	
	Bunn 50	contracted 50	Bunn 65	contracted 65
a (Å)	15.47 (15.62)	15.29 (15.02)	15.17 (15.62)	15.18 (15.02)
b (Å)	30.27 (30.24)	30.78 (30.24)	30.25 (30.24)	30.01 (30.24)
c (Å)	10.98 (11.02)	10.87 (10.82)	10.94 (11.02)	10.92 Å (10.82)
α (deg)	89.6 (90.0)	89.9 (90.0)	91.0 (90.0)	89.2 (90.0)
β (deg)	90.5 (91.4)	90.6 (91.2)	90.6 (91.4)	91.8 (91.2)
γ (deg)	89.5 (90.0)	89.9 (90.0)	92.1 (90.0)	90.4 (90.0)
vol. (Å^3)	5141.2 (5203.7)	5115.2 (4913.5)	5015.8 (5203.7)	4971.7 (4913.5)
ρ (g/mL)	1.37 (1.34)	1.37 (1.40)	1.40 (1.34)	1.41 (1.40)

[a] The values in parentheses are those of the starting models.

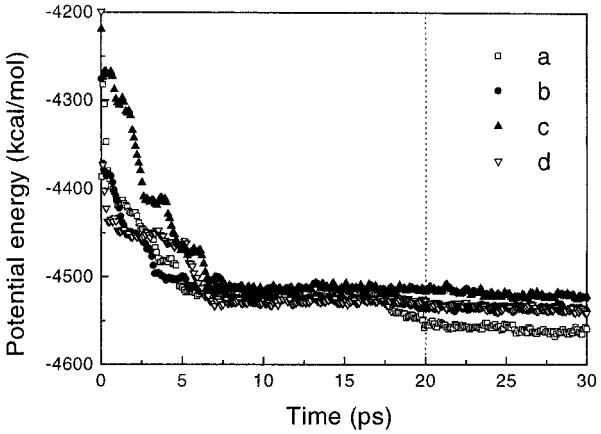

Figure 4. Potential energy for the four different models after a 30 ps *NVT* simulation: (a) Bunn 50, (b) Contracted 50, (c) Bunn 65, and (d) contracted 65 models. The vertical dashed line separates equilibration and data collection time frames. For clarity, only data for 100 fs intervals are shown.

oxygens is eliminated, most of the hydroxyls form intermolecular hydrogen bonding to the other chain in the unit cell, or to those in adjacent unit cells. Some of them can also form intramolecular hydrogen bonds to isotactic neighbors, such that all the hydroxyls can be

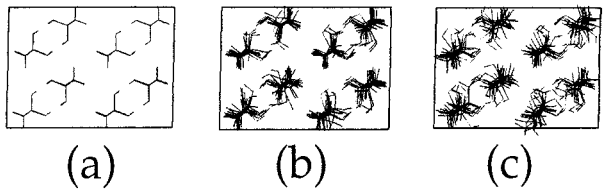

Figure 5. Snapshots of Bunn 50 model viewed along the *b* direction: (a) starting model, (b) model after molecular mechanics minimization, and (c) model after 30 ps as a *NVT* ensemble.

hydrogen bonded. Thus, the lattice dimensions are determined by a compromise between the interchain attractions due to hydrogen bonding and the van der Waals repulsions. When the S-diad ratio is increased, the two effects balance out at a lower interchain separation, i.e., the lateral unit cell dimensions decrease.

Constant Pressure and Temperature (*NPT*). It would be expected that two structural models (Bunn and contracted) constructed using the same nonidentical random sequences would converge to the same unit cell dimensions in simulations done at constant pressure and temperature. Table 6 shows the unit cell dimensions for the four different models before and after *NPT*

simulation. It can be seen that the predicted unit cell dimensions for the atactic models are larger those for the 65% S-diad models. The unit cell for the contracted 50 model has expanded and has dimensions close to the starting values for the Bunn 50 model. Meanwhile, the Bunn 65 model contracted toward the contracted 65 model. The calculated densities for the atactic and 65% syndiotactic models are ∼1.37 and ∼1.40 g/mL, respectively, which are close to the observed densities and those calculated from the X-ray data.

Conclusions

X-ray analysis showed that an increase in the syndiotacticity of PVA leads to contraction of the lateral unit cell dimensions, and to formation of larger crystallites with less distortions. Molecular mechanics simulations failed to predict the existence of contracted unit cell of 65% syndiotacticity PVA, probably due to inability to reach global minima. However, molecular dynamics simulations at 298 K showed that atactic PVA favors the larger unit cell (that proposed by Bunn), whereas PVA with 65% S-diad content preferred the observed contracted unit cell dimensions. The driving force for lateral unit cell contraction at 65% syndiotacticity appears to be the formation of shorter and thus stronger intermolecular hydrogen bonds. In the latter structure, the chances that adjacent monomers have opposite tacticity is ∼2:1, compared to 1:1 in the 50% model, and consequently the balance between hydrogen-bonding attraction and steric repulsion occurs when the chains are closer together, i.e., at a higher density.

References and Notes

(1) Bunn, C. W. *Nature* **1948**, *161*, 929.

(2) Sakurada, I.; Fuchino, K.; Okada, N. *Bull. Inst. Chem. Res. Kyoto University* **1950**, *23*, 78.

(3) Bunn, C. W.; Peiser, H. S. *Nature* **1947**, *161*, 159.

(4) Nitta, I.; Taguchi, I.; Nishimaki, S.; Sekiya, T. *Annu. Rep. Inst. Text. Sci. Japan* **1954**, *8*, 48.

(5) Nitta, I.; Taguchi, I.; Chatani, Y. *Annu. Rep. Inst. Fiber Sci.* **1957**, *10*, 1.

(6) Mochizuki, T. *Nippon Kagaku Zasshi* **1960**, *81*, 15.

(7) Mochizuki, T. *J. Chem. Soc. Jpn.* **1960**, *81*, 6.

(8) Tsuboi, K.; Mochizuki, T. *J. Polym. Sci.* **1963**, *B-1*, 531.

(9) Takahashi, Y. *J. Polym. Sci., Polmy. Phys. Ed.* **1997**, *35*, 193.

(10) Marten, F. L. In *Encyclopedia of Polymer Science and Engineering*, 2nd ed.; Mark, H. F., Bikales, N. M., Overberger, C. G., Menges, G., Eds.; Wiley-Interscience: New York, 1989; Vol. 17, p 167.

(11) Masuda, M. In *Polyvinyl Alcohol: Developments*; Finch, C. A., Ed.; Wiley: New York, 1992; p 403.

(12) Nakamae, K.; Nishino, Y.; Ohkubo, H.; Matsuzawa, S.; Yamaura, K. *Polymer* **1992**, *33*, 2581.

(13) Fukunishi, Y.; Aidyarna, A.; Sato, T.; Sano, H.; Ohmory, A. US Patent 5,238,995, 1993.

(14) Sakurada, I.; Ito, T.; Nakamae, K. *J. Polym. Sci.* **1966**, *C15*, 75.

(15) Tashiro, K.; Kobayashi, M.; Tadokoro, H. *J. Macromol. Sci.* **1977**, *10*, 731.

(16) Lyoo, W. S.; Blackwell, J.; Ghim, H. D. *Macromolecules* **1998**, *31*, 4253.

(17) Lyoo, W. S.; Ha, W. S. *J. Polyrn. Sci., Polym. Chem. Ed.* **1997**, *35*, 55.

(18) Hosemann, R.; Wilke, W. *Makromol. Chem.* **1968**, *118*, 230.

(19) Clark, M.; Cramer, R. D., III; Van Opdenbosch, N.; *J. Comput. Chem.* **1989**, *10*, 982.

(20) *Discover 2.9.8/96.0/4.0.0 User Guide*; Molecular Simulations Inc.: San Diego, CA, 1996.

MA9908402